Deep Subwavelength Terahertz Waveguides Using Gap Magnetic Plasmon

Atsushi Ishikawa,[1] Shuang Zhang,[1] Dentcho A. Genov,[1] Guy Bartal,[1] and Xiang Zhang[1,2,*]

[1]*NSF Nanoscale Science and Engineering Center (NSEC), 5130 Etcheverry Hall, University of California, Berkeley, California 94720-1740, USA*

[2]*Materials Sciences Division, Lawrence Berkeley National Laboratory, 1 Cyclotron Road, Berkeley, California 94720, USA*

(Received 6 September 2008; published 28 January 2009)

We propose a novel subwavelength terahertz (THz) waveguide based on the magnetic plasmon polariton mode guided by a narrow gap in a negative permeability metamaterial. Deep subwavelength waveguiding ($<\lambda/10$) with group velocities down to $c/21.8$ is demonstrated in a straight waveguide, a 90° bend, and a splitter. The proposed waveguiding system inherently has no cutoff for any core width and height, paving the way toward the deep subwavelength transport of THz waves for integrated THz device applications.

DOI: 10.1103/PhysRevLett.102.043904 PACS numbers: 42.25.Bs, 42.82.Et, 71.45.Gm, 78.20.Bh

Confining and steering electromagnetic (EM) waves at dimensions much smaller than the wavelength are of great importance for miniaturization of optical-integrated devices and improvement of the spatial resolution in optical imaging. Because of the diffraction limit, the size of an optical beam cannot, in general, be smaller than half of the wavelength in the host medium. In 1997, Takahara *et al.* showed that utilization of surface plasmon polaritons (SPPs), the surface modes at the metal-dielectric interfaces, had the potential to meliorate the diffraction limit in waveguides [1,2]. Subsequently, a variety of sub-diffraction-limit plasmonic waveguides capable of delivering EM energy have been demonstrated in the optical frequency region [3–5].

Terahertz (THz) technology is now drawing increasing attention due to its applications in biochemical sensing, security detection, and high-speed communication. To realize such applications, an easily accessible guided mode with highly localized EM fields is required. However, in the THz region where metal resembles a perfect electric conductor (PEC), the EM fields of SPP hardly penetrate into the metal, instead extend hundreds of wavelengths into the dielectric medium [6]. Although it has been demonstrated that SPP-like surface modes can be excited even on a PEC slab by introducing subwavelength holes on its surface [7,8], strong confinement and guiding of THz waves in the deep subwavelength scale ($<\lambda/10$) remains a major challenge.

Recently, the discovery of a new class of artificial materials, referred to as ''metamaterials'', has introduced a new paradigm in electromagnetism, where the optical properties of an artificial material can be designed at will [9–11]. These capabilities, supported by the advances in micro- or nanofabrication technologies, bring various unprecedented optical functionalities into reality [12–14]. Of special interest are magnetic metamaterials that can extend the magnetic responses to THz and even optical frequencies, well beyond the limit of what natural materials offer [15,16]. While these magnetic activities have not been well appreciated, they could provide unique EM configurations to manipulate the light more efficiently [17]. In this letter, we utilize a magnetic metamaterial in conjunction with a parallel-metal-plate waveguide to realize two-dimensional (2D) confinement and guiding of THz waves in the deep subwavelength scale.

In Fig. 1(a), parallel metal plates, also known as gap plasmon waveguides [18], can confine light and THz waves within a deep subwavelength one-dimensional (1D) gap. Since this confinement is electric-field-mediated, it can occur only along the x (electric field) direction, while in the y (magnetic field) direction, the beam size of the guided wave is still diffraction limited. On the other hand, a gap in a negative permeability material provides the magnetic boundary condition for magnetic-field-mediated confinement, as shown in Fig. 1(b). In analogy to SPPs, negative permeability materials can support surface mag-

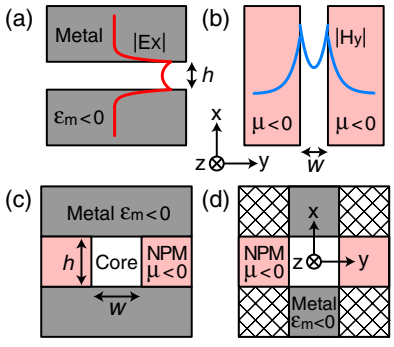

FIG. 1 (color online). (a) Parallel metal plates for the electric-field-mediated confinement in the x direction, and (b) a gap in a negative permeability material for the magnetic-field-mediated confinement in the y direction. (c) A 2D confined subwavelength THz waveguide consisting of a vacuum core and negative permeability metamaterial (NPM) claddings between the metal plates, and (d) its approximate analytical model to derive the dispersion relations of the guided mode, Eqs. (1)–(5).

netic plasmon polaritons (MPPs), which are transverse electric (TE) waves with the electric field E_x parallel to the material-vacuum interface [19]. When the gap width w is small enough, the MPPs excited at each interface are coupled, resulting in symmetric and antisymmetric gap MPP modes, defined by the E_x symmetry along the y direction. The symmetric mode, which has no cutoff in the zero gap-width limit, can be used for the confinement in the y direction (perpendicular to E_x). Based on this idea, we develop a novel subwavelength THz waveguide by incorporating a negative permeability metamaterial as claddings between the metal plates, as shown in Fig. 1(c). The proposed structure inherently has no cutoff for any core width and height, thus realizing 2D strong confinement in the deep subwavelength core.

We first derive the Marcatili's approximate analytical model shown in Fig. 1(d) for the dispersion relations of the guided wave that is strongly confined in the vacuum core [Eq. (3)] in two dimensions [20]: electric plasmon confinement along the x direction [Eqs. (1) and (4)] and magnetic plasmon confinement along the y direction [Eqs. (2) and (5)]. The EM fields are assumed to be negligible in the meshed corner regions.

$$\tanh(\kappa_x h/2) + (\gamma_x/\varepsilon_m\kappa_x) = 0 \quad (1)$$

$$\tanh(\kappa_y w/2) + (\gamma_y/\mu\kappa_y) = 0 \quad (2)$$

$$\kappa_x^2 + \kappa_y^2 = k_z^2 - (\omega/c)^2 \quad \text{(core)} \quad (3)$$

$$\gamma_x^2 = k_z^2 - \kappa_y^2 - \varepsilon_m(\omega/c)^2 \quad \text{(metal)} \quad (4)$$

$$\gamma_y^2 = k_z^2 - \kappa_x^2 - \mu(\omega/c)^2 \quad \text{(metamaterial)}, \quad (5)$$

where ε_m and μ are the metal permittivity and the metamaterial permeability, k_z is the propagation constant, and κ_x and κ_y, γ_x, and γ_y are the attenuation constants in the core, metal, and metamaterial. In the THz region, the PEC approximation ($\mathrm{Re}[\varepsilon_m] \to -\infty$) can be applied, resulting in $\kappa_x \to 0$ and $\gamma_x \to \infty$; thus, Eqs. (1)–(5) are reduced to the 1D gap MPP mode problem. Taking into account that the metamaterial can be anisotropic, we obtain

$$\tanh(\kappa_y w/2) + (\gamma_y/\mu_z\kappa_y) = 0 \quad (6)$$

$$\kappa_y^2 = k_z^2 - (\omega/c)^2 \quad \text{(core)} \quad (7)$$

$$\gamma_y^2 = (\mu_z/\mu_y)k_z^2 - \varepsilon_x\mu_z(\omega/c)^2 \quad \text{(metamaterial)}, \quad (8)$$

where ε_x, μ_y, and μ_z are the permittivity and permeabilities of the metamaterial. An inspection of Eq. (6) reveals that a gap MPP can exist in such a system provided the permeability of the metamaterial along the propagation direction (μ_z) is negative. Concurrently, to realize 2D guiding of THz waves in the y-z plane, a system with in-plane isotropic properties is desired; for this purpose, we designed a metamaterial made of an array of metal-dielectric-metal magnetic resonators [16]. As shown in Figs. 2(a) and 2(b), each magnetic resonator consists of a high-dielectric material (ε_1) sandwiched between two metal plates. The resonators are stacked along the x direction and arrayed in the y-z plane. Another low-dielectric material (ε_2) is used to separate the resonators in the x direction.

The metamaterial was numerically investigated using a finite-difference time-domain (FDTD) software package (CST Microwave Studio). In the calculation, silver is chosen for metal (ε_m), and $Ba_2Nd_5Ti_9O_{27}$ and Benzocyclobutene, which are high- and low-permittivity dielectrics, are used as ε_1 and ε_2 media, respectively [21–23]. Figure 2(c) shows the real and imaginary parts of the retrieved effective permeability μ_z of the metamaterial. A magnetic resonance is clearly observed at 0.71 THz. In the shaded region from 0.71 to 0.85 THz, which are surface MPP (smpp) resonant frequencies $\omega_{\mathrm{smpp}}^{(1)}$ and $\omega_{\mathrm{smpp}}^{(2)}$, the resonator array exhibits a negative permeability below -1.0.

Next, we study the frequency-dependent wave propagations in the proposed structure shown in Fig. 1(c). The core

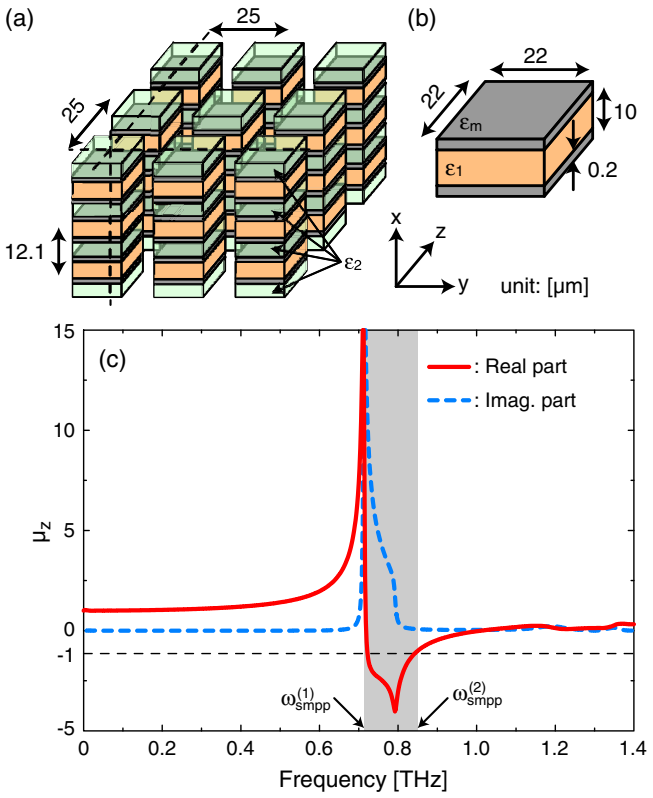

FIG. 2 (color online). (a) An array of magnetic resonators forming a metamaterial that exhibits isotropic negative permeability in the y and z directions and (b) a unit cell of the metal-dielectric-metal magnetic resonator. (c) Real (solid curve) and imaginary (dashed curve) parts of the retrieved μ_z of the metamaterial. The shaded region from $\omega_{\mathrm{smpp}}^{(1)}$ to $\omega_{\mathrm{smpp}}^{(2)}$ indicates the frequency range where $\mu_z < -1.0$.

width and height (38.0 μm) are deep subwavelength compared to the operating wavelength (~400 μm). Figure 3(a) shows the numerically retrieved dispersion relations for both the metamaterial cladding without the core (circle dots) and the gap MPP mode of the waveguide (triangle dots). The normalized spectrum of transmitted electric field E_x through the waveguide is shown in Fig. 3(b). A band gap opens in the dispersion of the metamaterial due to the negative magnetic response in the frequency range of 0.71 to 1.06 THz. Inside the band gap, three branches labeled as I, II, and III are formed by the gap MPP mode with dispersions closely following the analytical result

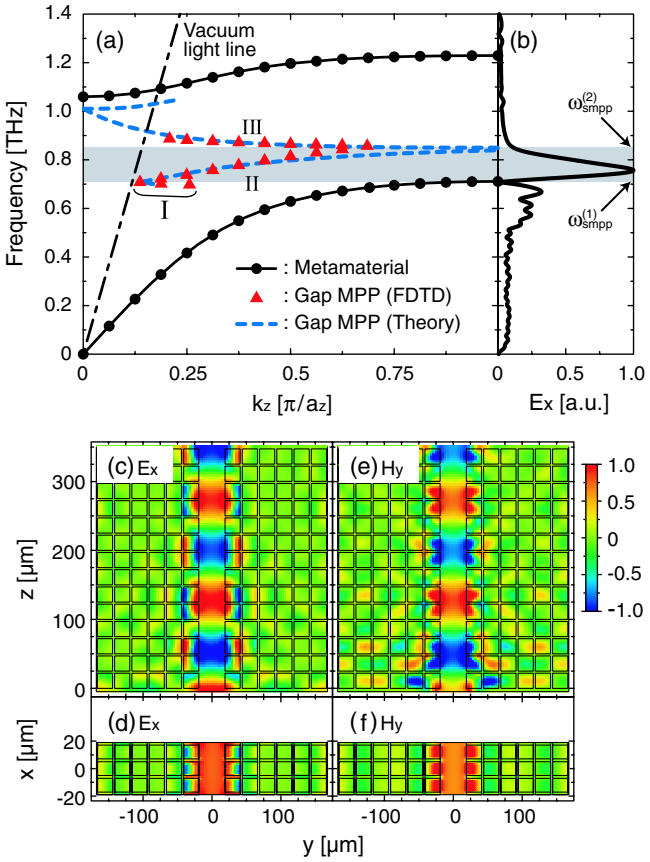

FIG. 3 (color online). (a) Numerically retrieved dispersion relations for both the metamaterial cladding (circle dots) and the gap MPP mode of the waveguide (triangle dots). The analytical result for the gap MPP mode based on Eqs. (6)–(8), dashed curve, is in good agreement with the FDTD result. No valid FDTD data were obtained above 0.9 THz because of weak transmission, while the analytical result predicts the existence of a fourth branch. The vacuum light line, dot-dashed line, is also shown for reference. (b) Corresponding transmission spectrum of the electric field E_x through the waveguide. The shaded region from $\omega_{\mathrm{smpp}}^{(1)}$ to $\omega_{\mathrm{smpp}}^{(2)}$ indicates the frequency range where $\mu_z < -1.0$. E_x distributions at 0.77 THz (branch II) in the (c) y-z plane at $x = 0$ μm and (d) x-y plane at $z = 260$ μm. (e) and (f) Corresponding H_y distributions in both planes. The metamaterial cladding in (c)–(f) indicated by the black lines consists of $3 \times 12 \times 14$ unit cells in the x, y, and z directions.

(dashed curve) based on Eqs. (6)–(8) and the effective optical constants as per Fig. 2(c). Three branches are divided by two surface MPP resonances at $\omega_{\mathrm{smpp}}^{(1)}$ and $\omega_{\mathrm{smpp}}^{(2)}$. In the shaded region where $\mu_z < -1.0$, the second branch, which contributes to the transmission peak centered at 0.77 THz, departs significantly from the light line and reaches asymptotically the upper edge of shaded region at large k_z. Note that at 0.85 THz, a large $k_z = 4.6k_0$ ($k_0 = \omega/c$ is the wave number in vacuum) is obtained, while a low group velocity of $c/21.8$ is achieved at 0.77 THz. Below and above the shaded region where $-1.0 < \mu_z < 0$, the first and third branches, which are quasibound modes with negative group velocities ($\partial\omega/\partial k_z < 0$) [18], fold back toward the lower and upper edge of the band gap at small k_z. Here, we focus on the second branch, since the first and third branches are strongly dissipative.

Figures 3(c) and 3(d) show E_x distributions at 0.77 THz in the y-z plane at $x = 0$ μm and in the x-y plane at $z = 260$ μm, for the x-polarized plane wave excitation from the lower end of the waveguide. The symmetric E_x profile of the coupled MPPs excited at each interface is clearly observed and strong confinement in the deep subwavelength core is achieved. In Fig. 3(d), the electric field is confined over the cross section of the core and penetrates only a single unit cell into the claddings. Similar confinement and waveguiding properties are also found for the magnetic field H_y shown in Figs. 3(e) and 3(f). At the interface, a strong magnetic field associated with the magnetic resonance is observed, generating the magnetic dipoles that couple to the MPPs. Following the confinement of the electric and magnetic fields, the EM energy flow in the waveguide is strictly concentrated in the core.

Despite the substantial imaginary part of μ_z at the considered frequency [Fig. 2(c)], a sufficient performance is still obtained since the absorption occurs only in a small area near the surface of the metamaterial claddings where the electric field is concentrated. For the considered configuration and operating frequency, we determined the propagation loss at 0.0064 dB/μm (2.5 dB/λ), which is on par with the subwavelength MPP transmission lines considered in the midinfrared region [24]. Furthermore, the numerical studies indicate that the propagation loss mainly results from the absorption in the high-dielectric material and not in the metal, which can be improved further by using low-loss dielectrics or by optimizing the operating frequency.

Finally, we show that the subwavelength waveguiding can be realized even in the presence of a sharp bend in the waveguide. Figures 4(a) and 4(b) show E_x distributions in the y-z plane of waveguides with a 90° bend and a splitter. In the calculations, the claddings are represented by an isotropic effective medium with $\mu = -7.79 + 0.86i$ at 0.77 THz. The core width w is 50.0 μm and the other geometric parameters are the same as above. The sub-

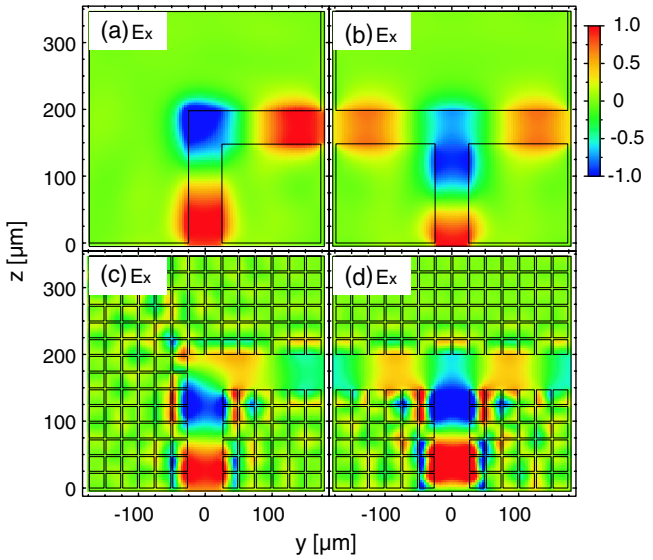

FIG. 4 (color online). Electric field E_x distributions in the y-z plane of waveguides with a 90° bend [(a) and (c)] and a splitter [(b) and (d)] at 0.77 THz. The claddings in (a) and (b) are modeled as an isotropic effective medium with $\mu = -7.79 + 0.86i$, whereas those in (c) and (d) consist of the magnetic resonator array, indicated by the black lines.

wavelength propagation is guided around the bend and splitter experiencing a low reflection. To quantitatively estimate the transmissivity through the bend, we consider two isometric waveguides. A comparison between the transmissions, with and without the bend, shows that the transmissivity through the bend reaches 96.5%. This is due to the improved impedance matching when the waveguide is sufficiently small compared to the wavelength and the bend can be considered as a junction between two transmission lines with the same characteristic impedance [25].

In Figs. 4(c) and 4(d), we show E_x distributions for the bend and splitter configurations by replacing the effective medium with the magnetic resonator array in the claddings. Although the wave is still guided around the bend, scattering is observed at the top corner where the electric field is strongly concentrated. As a result, only 23.8% transmissivity through the bend is observed. In the case of the splitter, the wave is well guided by the flat face of the resonator array and no significant scattering is observed at the T junction. Surprisingly, almost 63.5% impinging energy is transferred along the wings of the sharp T-junction. Since the splitter, which can be considered as a junction of three transmission lines with the same characteristic impedance Z, has an intrinsic reflection loss $R = |(2Z - Z)/(2Z + Z)|^2 = 11.1\%$, the scattering loss in the system can be estimated at up to 25.4%. This result suggests that the scattering loss in the 90° bend geometry, which results from the imperfection of the resonator array at the sharp corner of the bend, can be improved by properly arranging the resonator array around the corner.

In conclusion, we have presented a subwavelength THz waveguide based on the gap MPP mode guided by a vacuum core in a negative permeability metamaterial. Strong confinement and guiding of THz waves below the diffraction limit are demonstrated in a straight waveguide, a 90° bend, and a splitter. These unique wave-confining features based on unconventional EM configurations could open new route to highly efficient subwavelength THz devices. Such a waveguiding system can, in principle, operate at any frequency, given a magnetic material is obtained [26,27]. Hence, it may have great potential for optical applications, such as biomedical imaging, nanolithography, and ultrasmall optical-integrated circuit.

This work was supported by the U. S. Department of Energy (DOE) under Contract No. DE-AC02-05CH11231 and partly by the U. S. Army Research Office (ARO) MURI program 50432-PH-MUR. A. Ishikawa acknowledges support from the Japan Society for the Promotion of Science (JSPS).

*xiang@berkeley.edu

[1] J. Takahara *et al.*, Opt. Lett. **22**, 475 (1997).
[2] E. N. Economou, Phys. Rev. **182**, 539 (1969).
[3] S. A. Maier *et al.*, Nature Mater. **2**, 229 (2003).
[4] S. I. Bozhevolnyi *et al.*, Nature (London) **440**, 508 (2006).
[5] R. Oulton *et al.*, Nat. Photon. **2**, 496 (2008).
[6] K. Wang and D. M. Mittleman, Nature (London) **432**, 376 (2004).
[7] S. A. Maier *et al.*, Phys. Rev. Lett. **97**, 176805 (2006).
[8] C. R. Williams *et al.*, Nat. Photon. **2**, 175 (2008).
[9] A. Ishikawa, T. Tanaka, and S. Kawata, Phys. Rev. Lett. **95**, 237401 (2005).
[10] S. Zhang *et al.*, Phys. Rev. Lett. **95**, 137404 (2005).
[11] J. Valentine *et al.*, Nature (London) **455**, 376(2008).
[12] N. Fang *et al.*, Science **308**, 534 (2005).
[13] W. Cai *et al.*, Nat. Photon. **1**, 224 (2007).
[14] Z. Liu *et al.*, Science **315**, 1686 (2007).
[15] T. J. Yen *et al.*, Science **303**, 1494 (2004).
[16] G. Dolling *et al.*, Opt. Lett. **30**, 3198 (2005).
[17] T. Tanaka, A. Ishikawa, and S. Kawata, Phys. Rev. B **73**, 125423 (2006).
[18] J. A. Dionne *et al.*, Phys. Rev. B, **73**, 035407 (2006).
[19] J. N. Gollub *et al.*, Phys. Rev. B **71**, 195402 (2005).
[20] E. A. J. Marcatili, Bell Syst. Tech. J. **48**, 2071 (1969).
[21] P. B. Johnson and R. W. Christy, Phys. Rev. B **6**, 4370 (1972).
[22] P. Kuzel and J. Petzelt, Ferroelectrics **239**, 79 (2000).
[23] Dow Chemicals: http://www.dow.com/cyclotene/solution/highfreq.htm.
[24] H. Liu *et al.*, Phys. Rev. Lett. **97**, 243902 (2006).
[25] G. Veronis and S. Fan, Appl. Phys. Lett. **87**, 131102 (2005).
[26] W. Cai *et al.*, Opt. Express **15**, 3333 (2007).
[27] C. M. Krowne, Phys. Lett. A **372**, 2304 (2008).